Functional benefit of CRISPR-Cas9-induced allele deletion for *RYR1* dominant mutation

Mathilde Beaufils,[1] Margaux Melka,[1] Julie Brocard,[1] Clement Benoit,[2] Nagi Debbah,[1,2,3] Kamel Mamchaoui,[4] Norma B. Romero,[5] Anne Frédérique Dalmas-Laurent,[6] Susana Quijano-Roy,[7] Julien Fauré,[1] John Rendu,[1,8] and Isabelle Marty[1,8]

[1]University Grenoble Alpes, INSERM, U1216, CHU Grenoble Alpes, Grenoble Institut Neurosciences, 38000 Grenoble, France; [2]University Grenoble Alpes, TIMC, CNRS UMR5525, 38000 Grenoble, France; [3]University Grenoble Alpes, Departement de Pharmacochimie Moléculaire, CNRS UMR 5063, 38400 Saint-Martin-d'Hères, France; [4]Sorbonne Université, INSERM, Institut de Myologie, Centre de Recherche en Myologie, 75000 Paris, France; [5]Neuromuscular Morphology Unit, Institut de Myologie, Pitié-Salpêtrière Hospital, Sorbonne Université, 75000 Paris, France; [6]MH Unit, Lille University Hospital, 59000 Lille, France; [7]Neuromuscular Unit (NEIDF), Child Neurology and ICU Department, Raymond-Poincaré Hospital, (APHP University Paris-Saclay), 92380 Garches, France

More than 700 pathogenic or probably pathogenic variations have been identified in the *RYR1* gene causing various myopathies collectively known as "*RYR1*-related myopathies." There is no treatment for these myopathies, and gene therapy stands out as one of the most promising approaches. In the context of a dominant form of central core disease due to a *RYR1* mutation, we aimed at showing the functional benefit of inactivating specifically the mutated *RYR1* allele by guiding CRISPR-Cas9 cleavages onto frequent single-nucleotide polymorphisms (SNPs) segregating on the same chromosome. Whole-genome sequencing was used to pinpoint SNPs localized on the mutant *RYR1* allele and identified specific CRISPR-Cas9 guide RNAs. Lentiviruses encoding these guide RNAs and the *Sp*Cas9 nuclease were used to transduce immortalized patient myoblasts, inducing the specific deletion of the mutant *RYR1* allele. The efficiency of the deletion was assessed at DNA and RNA levels, and at the functional level after monitoring calcium release induced by the stimulation of the RyR1-channel. This study provides *in cellulo* proof of concept regarding the benefits of mutant *RYR1* allele deletion, in the case of a dominant *RYR1* mutation, from both a molecular and functional perspective, and could apply potentially to 20% of all patients with a *RYR1* mutation.

INTRODUCTION

Muscle stimulation at the neuromuscular junction induces membrane depolarization, activating a macromolecular protein complex known as the calcium release complex (CRC). This complex, composed of the plasma membrane voltage-sensitive calcium channel (dihydropyridine receptor [DHPR]) and the intracellular calcium channel (ryanodine receptor [RyR1]), allows intracellular calcium release, leading to muscle contraction.[1] The CRC's function relies on the cross-talk between its two main components: the DHPR, activated by membrane depolarization, and the RyR1, releasing calcium from the sarcoplasmic reticulum into the cytosol upon stimulation.[1] Mutations in the gene encoding the skeletal muscle ryanodine receptor *RYR1* result in altered intracellular calcium release through

various pathophysiological mechanisms, including gain of function, loss of function, and reduction in protein amount.[1–4] The human *RYR1* gene, spanning 150 kbp on chromosome 19, is transcribed into a 15-kbp mRNA corresponding to sequences of 106 exons.[5] All exons except the alternative exons 70 and 83 are indispensable. The functional RyR1 calcium channel is a homotetramer, with each monomer containing 5,037 amino acids in humans. Mutations in *RYR1* are distributed throughout the gene sequence,[6] with over 1,500 variations identified to date, accounting for dominant or recessive phenotypes (among which 700 are pathogenic or probably pathogenic, according to the American College of Medical Genetics classification[7]). *RYR1* mutations are responsible for various myopathies, including central core disease (CCD), multimini core disease (MmD), dusty core disease (DuCD), centronuclear myopathy (CNM), collectively referred to as RyR1-related myopathies (RyR1-RM). These mutations are the most commonly found in patients with congenital myopathy.[2,3,8] Patients typically present with muscle weakness of varying severity, from severe neonatal presentation with respiratory insufficiency to mild/isolated or generalized muscle weakness.[2] Mutations in the *RYR1* gene can also result in different triggered syndromes: malignant hyperthermia (MH) a hyperthermic and hypercontracture response triggered by anesthesia, and rabdomyolysis induced by exercise, stress, or heat.[9]

Currently, there is no treatment for RyR1-RM, and various therapeutic strategies are under exploration.[4] Gene therapy, although promising, faces challenges due to the *RYR1* coding sequence's size, unsuitable for a single viral vector packaging. In addition, truncating mutations with a protein that remains functional do not exist,[10] which makes so far gene transfer, potentially with a shorter version, not a
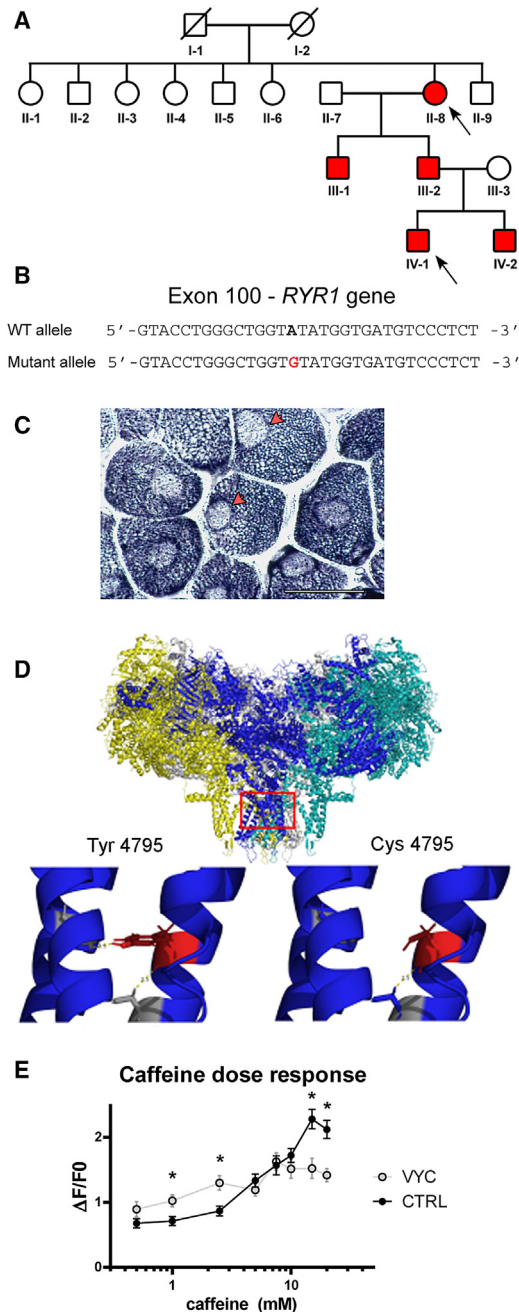

Figure 1. Description of the family and of the _RYR1_ mutation

(A) A dominant _RYR1_ neo-mutation has been identified in patient II-8,[17] resulting in the change of tyrosine 4796 for a cysteine. This mutation has been transmitted to the two sons, and to the two grandchildren, all being affected by central core disease (affected patients are in red). (B) At the DNA level, the mutation c.14387A>G is localized in exon 100 of _RYR1_ gene. (C) Histological analysis (NADH staining) shows the presence of cores (red arrows) in each muscle fiber of patient II-8, typical of central core disease. Scale bar, 50 μm. (D) The structure of rabbit RyR1 and the position of the mutation in the pore of the channel (on the rabbit sequence, mutation is Y4795C). In presence of a cysteine in position 4795, the number of hydrogen bonds with the nearby α-helix is reduced compared with tyrosine. The reduction in

possible option. Intervening at the mRNA level using antisense oligonucleotides or small interfering RNA (siRNA) has shown promising results both _in cellulo_[11] and _in vivo_.[12] However, these studies were limited to a single patient or family, as they targeted patient-specific mutations, making them overly personalized for widespread therapy. Gene editing using CRISPR-Cas9 is an active research field, with the potential to replace (thanks to homology directed repair [HDR] after DNA cleavage, or more recently thanks to base/prime editing) or delete (based on non-homologous end joining [NHEJ]) a mutant DNA.[13] However, HDR-based correction is not applicable to non-dividing muscle fibers, limiting its use for myopathies. Successful deletion of a DNA segment or point correction with base/prime editing has been achieved in skeletal muscle.[14–16] In this study, we show that CRISPR-Cas9-mediated DNA deletion in the _RYR1_ gene is a potential therapeutic strategy for dominant RyR1-RM. Instead of targeting the patient's mutation directly, we directed the nuclease cleavage to single-nucleotide polymorphisms (SNPs) present on the same allele, inducing the exclusive loss of function of the mutant allele. We show that this strategy induces the extinction of the mutant allele in patient cells and a functional improvement in the calcium release. This mutation-independent allele deletion provides _in cellulo_ proof of concept for the efficacy of CRISPR-Cas9 allele deletion in patients with dominant RyR1-RM.

RESULTS

Patient description

The c.14387A>G variation resulting in the change of the tyrosine 4796 for a cysteine (p.Y4796C) in exon 100 of the _RYR1_ gene has been previously identified in all the individuals of the family affected by a dominant form of RyR1-RM (Figures 1A and 1B).[17] This neo-mutation affects individual II-8, who has two affected sons and two affected grandsons (IV-1 and IV-2) and presents mild symptoms of CCD (walking ability maintained), associated with MH susceptibility, with typical images of cores at histological analysis of the muscle biopsy (Figure 1C). Her grandson, (patient IV-1), presented, as many classic dominant _RYR1_-mutated patients, with congenital hip dislocation that was treated by surgery. He acquired walking ability and developed a spinal deformity that did not require surgery. At 17 years of age, at his last visit, he remained ambulant, showed no contractures and had normal pulmonary function tests. He had a non-progressive scoliosis (Cobb angle of 40°) with overall good trunk balance. His brother (patient IV-2) presented with a more severe phenotype,

the interaction between these two helixes in the pore probably results in a reduction in the strength of the closing of the channel. (E) Mean peak of calcium release induced by caffeine stimulation on patient immortalized myotubes (VYC) or on control myotubes (CTRL), using Fluo-4 calcium imaging. For each concentration, values are presented as mean ± SEM of fluorescence variation measured on 85 to 170 myotubes. At low caffeine concentration (1 mM–2.5 mM), a significantly higher calcium release, characteristic of MH sensitivity, is observed in the VYC patient cells compared with CTRL cells, whereas at high concentration (>15 mM), a significantly lower calcium release is observed. Statistical analysis Student t test between CRTL and VYC at each concentration: 0.5 mM $p = 0.1077$, 1 mM $p = 0.0071$, 2.5 mM $p = 0.0019$, 5 mM $p = 0.2852$, 7.5 mM $p = 0.7634$, 10 mM $p = 0.2515$, 15 mM $p = 0.0005$, 20 mM $p < 0.0001$; *$p < 0.05$.

had congenital hip dislocation at birth, which required early surgery, and was never able to walk. He developed respiratory insufficiency and required bracing during childhood and spinal fusion at the end of the growth period. At his last clinical visit at 15 years of age, he had a moderately reduced vital capacity, without the need of nocturnal ventilator support (65% of normal values) and showed hip and knee flexion contractures.

The c.14387A>G; p.Y4796C mutation is localized within the pore of the channel (Figure 1D), and the presence of the cysteine results in a reduction of the hydrogen bonds between two α-helixes in the pore. Ectopic expression of an RyR1 channel with this mutation in HEK cells has shown that the mutated RyR1 channel is hypersensitive to caffeine stimulation and presents a gain of function with a calcium leak resulting in depletion of the calcium store,[17] leading to the associated diagnosis of MH susceptibility.[18] Primary myoblasts have been obtained from a muscle biopsy of patient II-8, and immortalized as described previously[19] by a double retroviral transduction (hTERT and Cdk4) followed by clonal selection. These myoblasts, so-called V-Y4796C or VYC cells, have been further used for the development of the proof of concept of the functional benefits of allele deletion. The hypersensitivity to caffeine stimulation of the mutant RyR1 has been confirmed on these myoblasts (Figure 1E), in straight line with the previously reported MH susceptibility associated with this mutation.[17]

Identification of the SNPs and gRNAs selection

It has been previously observed that one functional RYR1 allele is sufficient for a normal muscle function in humans. Indeed, in families with the recessive form of RyR1-RM, individuals who harbor one loss-of-function allele and one normal RYR1 allele have no clinical signs.[20] This has been further confirmed in mice heterozygous for an RYR1-KO allele that show no phenotype.[21] In addition, allele-specific gene silencing using siRNA has demonstrated a functional benefit in two mouse models with dominant RYR1 mutations resulting in CCD and MH.[12] The goal of the project was therefore to show that switching-off the mutant RYR1 allele while preserving the normal one was beneficial in muscle cells of a patient with a dominant form of RyR1-RM. The allele knockdown was induced using the SpCas9 nuclease, and a double cleavage that would result in the deletion of an essential part of the RYR1 gene associated to frameshift was designed. In order to develop a strategy that could further be applied to other mutations, the targets of nuclease were SNPs present on the same allele as the mutation, and not the mutation itself. We chose to target SNPs with a frequency >1% in order to develop a versatile tool that could be applied to other patients. The first step of the project was to identify the SNPs present on each allele, and to determine which ones could be used for the design of guide RNA (gRNA).

Whole-genome sequencing (WGS) was performed on DNA from patients II-8 and IV-1, allowing the identification of all the SNPs present in the two patients. Only the SNPs present in the RYR1 gene and shared by the two patients were further considered (Figure 2A). The SNPs with a frequency above 1%, present in the RYR1 gene at

a heterozygous state, were further used for the screening. From the 79 SNPs identified, we selected the 14 SNPs in which the SNP resulted in the formation of a SpCas9 protospacer-adjacent motif (PAM) NGG (Figure 2A). These 14 SNPs were therefore present only on the mutant RYR1 allele, and absent from the wild-type (WT) allele. SpCas9-targeted cleavage would theoretically result in a cleavage 3 bases upstream of the PAM sequence, and only on the mutant allele. Guide RNAs (gRNAs) were further designed on these SNPs/PAM (Figure 2B), and five gRNAs were selected. As our goal was to knock out specifically the mutant RYR1 allele, gRNAs were chosen to obtain two cleavage sites leading to deletion of at least one exon and a disruption of the reading frame in RYR1. Pairs of gRNAs were further formed and cloned in a lentiviral vector, to produce the so-called "Lenti-guides" as described before,[22] expressing the two gRNAs independently. Five pairs were selected to produce Lenti-G1 to Lenti-G5, resulting in deletion of 1–70 exons of the RYR1 gene (Figure 2C), from 1,740 bp to more than 90,000 bp.

Validation of the selected gRNA and clone production

Immortalized muscle cells from the patient (VYC cells) were transduced with two lentiviruses encoding respectively the SpCas9 (Lenti-Cas9) and one of the gRNAs pair (Lenti-G1 to 5), as described previously,[22] and 5 days later, the cells were transduced with a so-called Lenti-Killer[22] encoding a gRNA targeting the SpCas9 gene, in order to stop the nuclease production.[23] After a 7-day amplification, the cells were collected and the deletion in the RYR1 gene checked by PCR analysis of the targeted regions (Figures 3A and 3B; Table 1). Only Lenti-G2 resulted in a deletion in the RYR1 gene, visualized by PCR amplification of the corresponding DNA region in the whole cell population (Figure 3C). The experiments were thus further performed only with cells treated with Lenti-G2, corresponding to a deletion of the three exons 18–20 (deletion of 3,691 bp, Figure 2C). The respective amount of each amplification product on cells treated with lenti-G2 has been estimated to be 20% for the cleaved band and 80% of the non-cleaved band (the maximal possible amount for the cleaved band being 50%, and 50% for the non-cleaved band). The other Lenti-Gs (1, 3, 4, and 5) were no more used in this study, as no cleaved band was observed. A pool of cells treated with the three lentiviruses (Lenti-Cas9, Lenti-G2, and Lenti-Killer) in which the deletion of the chosen region has been evidenced by PCR was submitted to single-cell cloning by limited dilution. After amplification, each individual clone was checked for RYR1 gene editing using the same PCR amplification, followed by Sanger sequencing of the amplified region (Figure 3D). Two populations were clearly identified in the selected clones: edited clones (so-called ECs), presenting two bands after PCR amplification corresponding respectively to the WT allele and the deleted allele (such as EC-A, EC-B, and EC-C, Figure 3D), and non-edited clones (NECs) presenting only one band after PCR amplification resulting in amplification of the two unmodified alleles (such as NEC-A, NEC-B, and NEC-C, Figure 3D). The same quantification procedure of the respective amount of cleaved/non-cleaved DNA confirm in each edited clone the presence of one edited allele and one intact allele (respective amount cleaved-intact of 45/55 in EC-A, 44/56 in EC-B, and 47/53 in
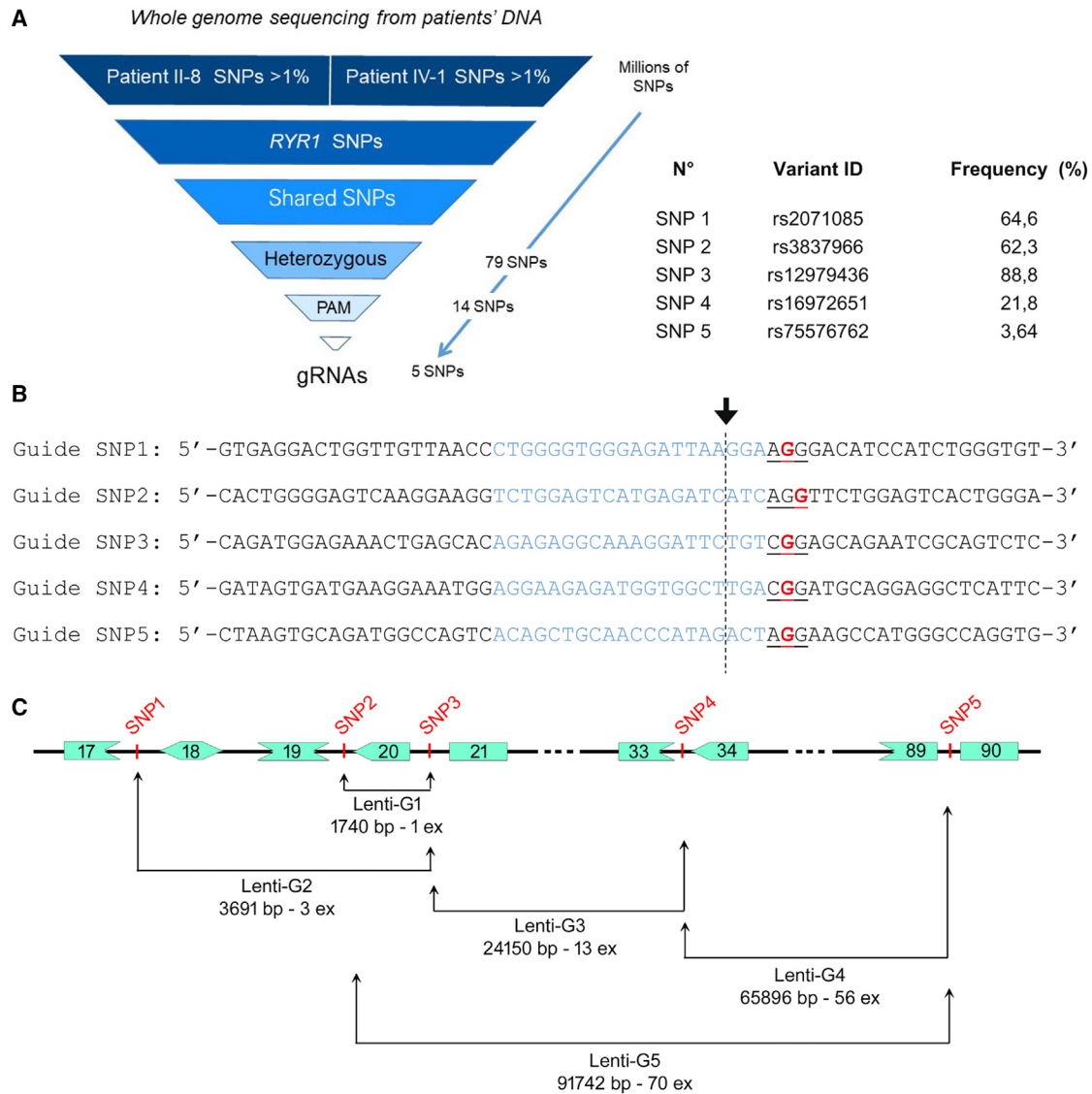
Figure 2. Pipeline for selection of the SNP and identification of gRNA

(A) Whole-genome sequencing has been performed on patient II-8 and patient IV-1 DNA, and the frequent SNPs in each patient's genome collected. The SNPs were further filtered to select only the ones present in the *RYR1* gene, and common to both patients, at heterozygous state. At this step, the 79 SNPs present in the *RYR1* gene only on the mutant allele were identified. After an additional selection, only the 14 SNPs creating an *Sp*Cas9 PAM (NGG) were used to select the best possible gRNAs using the CRISPOR tool (http://crispor.tefor.net/) based on specificity, efficiency, and predicted off-target. Only five SNPs further resulted in the identification of gRNA of top quality (based on MIT score and off-target prediction). In parallel, a dedicated script has been developed to perform automated SNP screening and selection (available at https://github.com/clbenoit/CutOneStrand), leading to selection of the same gRNA. The frequency of the five selected SNPs, determined using gnomAD v3.1.1 on January 11, 2023, and the variant ID is presented on the right. (B) The five best gRNAs corresponding to five heterozygous SNPs of the mutant *RYR1* allele were further used. Each SNP is represented in bold red, the PAM is underlined, and the corresponding gRNA is in blue. The *Sp*Cas9 cleavage site is represented by the arrow and the dashed line. (C) Pairs of gRNAs were further formed to produce lentiviruses called "Lenti-G" that lead to deletion of at least one exon and disruption of the reading frame. The localization of the selected SNP/gRNA is represented with reading frame of the surrounding exons, allowing visualization of the frameshift, and the size of expected deletion with each pair of guides.

EC-C). For the edited clones, the Sanger sequencing confirmed a cleavage 3 bp upstream of the PAM and the deletion of the sequence in-between (Figure 3E), corresponding to deletion of intron 17 to intron 20. After PCR amplification of the regions encompassing each guide and Sanger sequencing, no deletion was observed in NECs. For the subsequent molecular and functional characterization, three edited clones (EC-A, EC-B, and EC-C) and three non-edited clones (NEC-A, NEC-B, NEC-C) were selected.
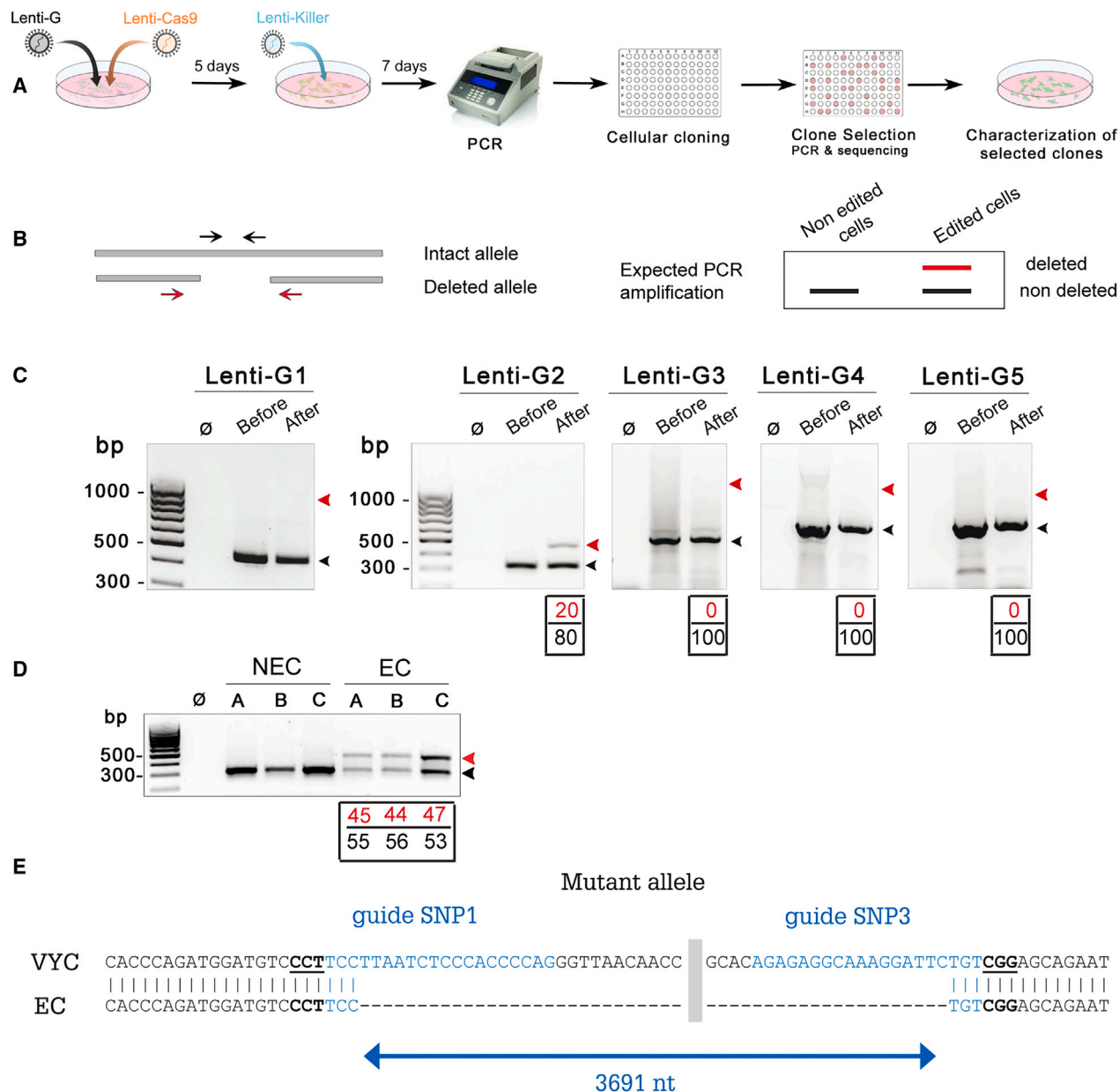
Figure 3. Validation of the gRNA and selection of clones

(A) Workflow of the whole treatment of the cells to obtain edited cell lines. The patient's cells were treated with two lentiviruses (Lenti-G1 to 5 and Lenti-Cas9), and 5 days later the nuclease was inhibited by Lenti-Killer. After 7 days, the edition efficiency was analyzed for each gRNA pair by PCR. When edition was observed, the cells were cloned, amplified, and the editing controlled in each clone by PCR and sequencing. The functional consequence of *RYR1* edition was further analyzed by calcium imaging. (B) For each Lenti-G (gRNA pair), primers were designed to amplify exclusively the intact allele (primer within the two cleavage sites, black arrows) or the deleted allele (primer on both side of the cleavage sites, red arrows) (Table 1). The red primers could theoretically amplify both the intact and the deleted alleles, but the fragment on the intact allele was too large to be amplified with the same PCR settings. The scheme on the right depicts the expected results of PCR amplification on edited and non-edited cells with the two sets of primers used together. Note that the red primers for the amplification of the deleted allele have been designed to produce a larger PCR product than the one corresponding to the intact allele produced with the black primers. (C) PCR amplification of the edited (red primers) and non-edited allele (black primers) for each Lenti-G. PCR amplification has been performed without DNA (ø), or with DNA extracted from the patient's cells before and after treatment with Lenti-G and Lenti-Cas9. The DNA segment corresponding to the red primers cannot be amplified in the intact allele because it is too large. The size of the amplicons are respectively for lenti-G1: 440 bp (intact allele, black arrow) and 985 bp (deleted allele, red arrow); for lenti-G2 314 bp (intact allele, black arrow) and 507 bp (deleted allele, red arrow); for lenti-G3 470 bp (intact allele, black arrow) and 1,266 bp (deleted allele, red arrow); for lenti-G4 659 bp (intact allele, black arrow) and 1,145 bp (deleted allele, red arrow); for lenti-G5 619 bp (intact allele, black arrow) and 1,074 bp (deleted allele, red arrow). The relative amount (in %) of each band (upper box for deleted band in red and lower box for intact band in black) after PCR

(legend continued on next page)

Molecular characterization of the clones

In order to confirm the consequence of DNA deletion at the molecular level, and to confirm the deletion of the mutant allele, analysis of *RYR1* mRNA in the three ECs and the three NECs was performed and compared with control cells (CTRL, immortalized myoblasts from a non-affected individual) and VYC cells. RyR1 being expressed only in differentiated muscle cells, mRNA was extracted from myotubes produced for each clone after 7 days in differentiation. PCR amplification and NGS sequencing of the region encompassing the mutation demonstrated that in the CTRL, only a normal transcript is observed whereas in VYC cells, the WT and the mutant transcript are present in equivalent amounts (Figure S1). In the ECs the relative amount of mutant transcript was reduced and the WT was increased, whereas in the NECs as in the initial patient's cells VYC, both the normal and the mutant transcripts were detected in equivalent amount (Figure 4A). In the edited clones, the deletion of the DNA region between the two guides led to nonsense-mediated decay (NMD) of the mutant allele (reduced from 50% to 33%), as estimated by quantification of the NGS reads corresponding to WT or mutant transcript (histogram 4A, right). No other transcript was observed. After DNA cleavage at the two gRNA sites, not only deletion of the DNA fragment could occur, but also segmental inversion that would result in a frameshift leading to disruption of the allele. The presence of a segmental sequence inversion between the two cleavage sites has been checked by PCR and Sanger sequencing and was not detected. The clones were further characterized at the protein level, using quantitative western blot. In order to be able to compare their function, their differentiation ability was estimated by the quantification of the amount of myosin heavy chain (MYHC, expressed in differentiated myotubes) compared with glyceraldehyde-3-phosphate dehydrogenase (GAPDH) in each clone. No significant difference was observed between the ECs, the NECs, and the initial patient cells (Figure 4C, left histogram). The relative amount of RyR1 compared with MYHC was also estimated, and no difference between the EC and NEC clones was observed (Figure 4C, right histogram). The expression level of Cas9 was checked, in order to evaluate if after the whole procedure, and the addition of the Lenti-Killer, the Cas9 protein expression has been abolished as expected (Figure 4D). The Cas9 protein was not detected in any clones, EC or NEC.

Control of selectivity of the cleavage sites

The selected gRNAs have been chosen based on their individual predicted maximal efficiency and their minimal off-target (OT) cleavages. Therefore, none of the selected gRNAs presented any predicted OT cleavage with 0 or 1 mismatch. To further screen for potential OT Cas9 cleavages, at least 10 DNA regions encompassing possible OT cleavage sites with two or more mismatches, predicted by at least two different types of software, were amplified by PCR and sequenced. Three different types of software were used to identify the putative OT sites for each gRNA (gRNA1 and gRNA2 for *RYR1*, and g-Killer for *Cas9*): Benchling (https://benchling.com/), CRISPOR (http://crispor.tefor.net/), and Cas-OFFinder (http://www.rgenome.net/cas-offinder/). For each gRNA the most probable first 10 to 13 sites predicted by at least two types of software were further selected for in-depth analysis (Figure 5A). A total of 36 predicted OT sites were therefore analyzed by PCR amplification (localization and primers presented in Table 2) followed by sequencing for each of the three ECs and the three NECs. Among those, two sites corresponding to intergenic regions (OT11 and OT14) have not been successfully amplified and sequenced even after changing the primers. No OT cleavages were identified in any of the predicted regions, in any of the clones (Figure 5B). In addition, using another cell line that has the two heterozygous SNPs on one allele (the AB1190 cell line, produced from another non-affected individual), we confirmed that the cleavage is observed when the two SNPs are present (AB1190 cells, Figure 5C), but no cleavage is observed when the two SNPs are not present (Figure 5C), such as in the CTRL cell line.

Functional characterization of the selected clones

In the normal function of myotubes, membrane depolarization activates the voltage-activated calcium channel dihydropyridine receptor, which in turn activates the RyR1 by a direct molecular interaction between the two proteins,[24] leading to a massive intracellular calcium release performed via RyR1. Therefore, to study the function of RyR1 after editing, calcium release has been studied using calcium imaging with the calcium-sensitive dye Fluo-4 in the three ECs and the three NECs, compared with the initial patient cells VYC and CTRL cells. The mutation Y4796C re-expressed in HEK cells has previously been shown to result in a leaky RyR1, with hypersensitivity to caffeine and reduction in the amount of calcium stored into the sarcoplasmic reticulum.[17] The effect of the mutation has now been directly studied in patient's cells. Membrane depolarization induced by addition of KCl 140 mM confirmed the reduction in the amount of calcium (reduction in peak amplitude and reduction in the area under the curve) in VYC cells compared with CTRL cells (Figure 6). The deletion of the mutant *RYR1* allele in the ECs induced a significant increase in the amplitude of the calcium release (Figure 6B), which became non-significantly different from CTRL. The amount of calcium released, represented by the area under the curve, also increased but remained significantly different from CTRL (Figure 6C). Each individual EC had the same behavior (Figure S2). In contrast, the NECs remained non-significantly different from the patient's cell VYC

amplification on treated cells quantified by densitometry with Image Lab (Bio-Rad) is presented below each lane. (D) PCR amplification of the edited and non-edited allele (red and black primers described above) after DNA purification of each individual clone. The edited clones (so-called ECs) present two bands after PCR amplification corresponding to the WT allele (lower band) and the deleted allele (upper band) (EC-A, EC-B, EC-C, …), and the non-edited clones (NECs) present only one band after PCR amplification resulting of amplification of the two alleles (NEC-A, NEC-B, …). The relative amount (in %) of each band (deleted in red or intact in black) after PCR amplification on EC quantified by densitometry with Image Lab (Bio-Rad) is presented below each lane. (E) Sanger sequencing of the deleted PCR band produced in edited clones with the red primers, aligned on the sequence of the patient cells VYC. The sequence of each guide is represented in blue, and the PAM is underlined. The gray zone corresponds to the sequence deleted not represented in the VYC sequence. The Cas9 cleavage occurs 3 bp upstream of the PAM.

Table 1. Primers for PCR amplification after cleavage with lenti-G1 to 5

Lenti G1	Forward (5′-3′)	Reverse (5′-3′)	Size
Intact allele (black)	GACACTATGACTGCCCGGTGACCT	ACAGGCATGAACGATGGCACCC	440 bp
Deleted allele (red)	CGTGACTCCAGACTCTTTCCA	CACGGAGGAACAAACTGAGG	985 bp
Lenti G2	Forward (5′-3′)	Reverse (5′-3′)	Size
Intact allele (black)	TACGGGAGCATCCAAGGGAGCA	AACAGGGAAGAAGAGCCCGTCCA	314 bp
Deleted allele (red)	ACTCATGTGACCCTCCCTCAGCCT	TCCCTGAGACTGCGATTCTGCTCC	507 bp
Lenti G3	Forward (5′-3′)	Reverse (5′-3′)	Size
Intact allele (black)	TGCAGATGCTGATGCCAGTGTCCT	GTGTTGATGTGGGTCTGGCTCCCT	470 bp
Deleted allele (red)	ACTTTGGATGGCCAGGCGTGGT	AGGTCACCGGGCAGTCATAGTGTC	1,266 bp
Lenti G4	Forward (5′-3′)	Reverse (5′-3′)	Size
Intact allele (black)	TTGTGCCTGTGCTCAAGCTCGTG	ATGGGTGGATGGAAAGGCTGGTGG	659 bp
Deleted allele (red)	AGCACAGTGAGAACCCGTCTCCAC	AGGATGTGAGGCTCAGGTTCAGGG	1,145 bp
Lenti G5	Forward (5′-3′)	Reverse (5′-3′)	Size
Intact allele (black)	AGTCCTCCACCAGCCTTTCCATCC	TGCTCCACTGCACTCTTCAGCCT	619 bp
Deleted allele (red)	TACGGGAGCATCCAAGGGAGCA	GGATGTGAGGCTCAGGTTCAGGGA	1,074 bp

(Figures 6B and 6C), and all the three individual NEC clones behave identically (Figure S2).

Direct RyR1 stimulation by its agonist caffeine confirmed the hypersensitivity of patient cells VYC compared with CTRL cells and the normalization of this hypersensitivity by RyR1 editing (Figures 6D, 6E, and 6F). The three ECs had the same behavior, and the three NECs behave also identically (Figure S2).

All these functional experiments, therefore, demonstrate that deletion of the mutant *RYR1* allele in the edited clones reverses, at least partially, the abnormal calcium handling of the patient's cells.

DISCUSSION

As of 2022, more than 700 variants in the *RYR1* gene have been classified as pathogenic or likely pathogenic, making it the most common gene associated with congenital myopathy and MH.[10] Over the period 2012–2022, during the genetic diagnosis performed in the Grenoble University Hospital, 161 pathogenic or likely pathogenic variations have been identified in the *RYR1* gene, with 120 variations of dominant transmission (RyR1-RM and MH). Unfortunately, there is currently no treatment available for any *RYR1* mutation. Among these variants, about 20% are associated to a dominant form of RyR1-RM and 54% to MH. The therapeutic approach presented here holds potential for application to any dominant pathology in which one functional allele is sufficient (MH and RyR1-RM, which reach about 75% of the variants). Searching the Online Mendelian Inheritance in Man (OMIM) database, we identified a list of 571 genes associated with dominant mutations (Table S1), for which the strategy presented here could potentially apply if one allele is sufficient.

Whereas the complete knockout (KO) of the *RYR1* gene in mice has been reported to be lethal at birth,[25] experimental evidence has demonstrated that a single WT allele is sufficient for normal muscle function. Specifically, heterozygous animals from an RyR1 KO mouse line showed that protein production with a single allele reaches 85% of the normal amount produced in WT animals.[21] Moreover, mice with an RyR1 amount of 70% exhibited no muscle strength deficit, as observed in an inducible RyR1-KO mouse model.[26] In humans, the presence of a null allele along with a normal *RYR1* allele has not been associated with muscle weakness, as seen in parents of patients with a recessive RyR1-RM.[20] Therefore, the deletion of a mutant allele, leaving a single functional allele alone, will likely represent an effective therapeutic solution.

The therapeutic strategy developed here is based on the use of two guides targeting allele-specific and frequent SNPs. In a similar approach, a high mutant allele specificity for mutations in *TGFBI* gene linked to corneal dystrophy has already been demonstrated *in vitro*, with one gRNA targeting a heterozygous SNP, the second one targeting an intronic region present on both alleles.[27] Thus, with two allele-specific gRNAs targeting the mutant *RYR1* allele, an even higher specificity with preservation of the WT allele was expected. Further experiments in different unrelated immortalized cell lines have confirmed that when one of the two targeted SNPs is absent, no deletion in the *RYR1* gene is observed, and the deletion occurs only when the two SNPs are present. This result strengthens the notion that when the two SNPs are absent, no deletion in the *RYR1* gene is observed, and conversely, when the SNPs are present, the deletion is observed, linking therapeutic efficiency to the presence of the SNPs rather than to the specific mutation. Consequently, patients with the same SNPs associated with a mutant allele of *RYR1* could potentially benefit from a similar therapeutic approach, regardless of the specific mutation on the gene, as long as the second functional allele lacks one of the two targeted SNPs. As these SNPs are frequent (respective frequency 64.6% for SNP1 and 88.8% for SNP3), the eventuality of their simultaneous presence on the same chromosome 19 together with a *RYR1* mutation, with at least one of the two being
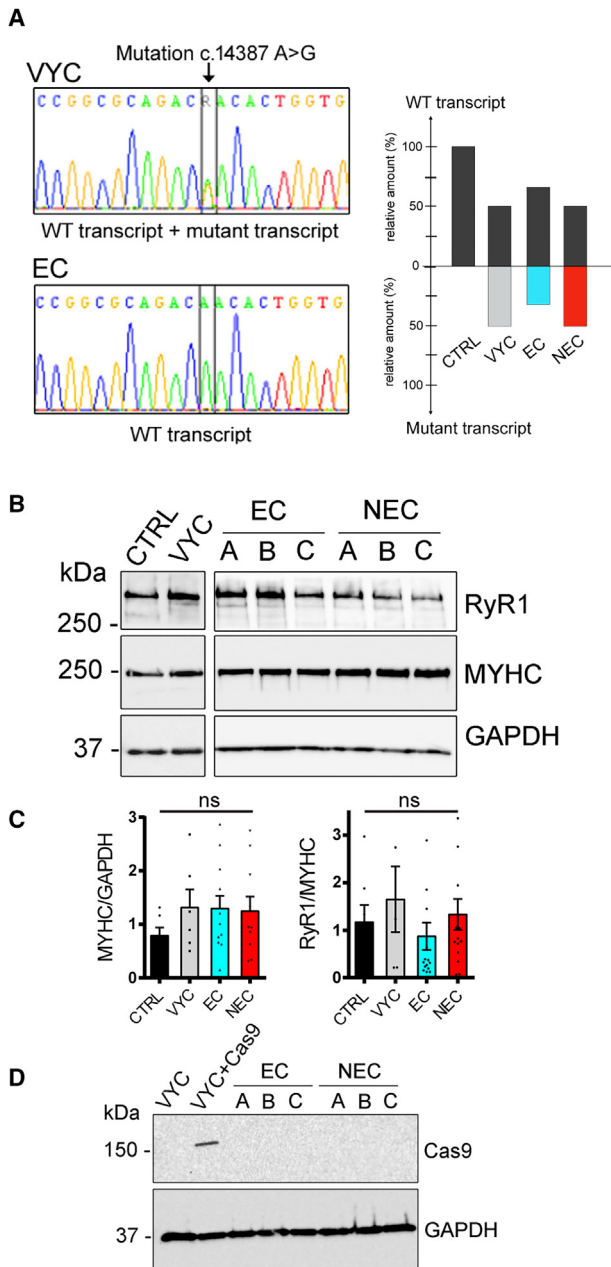
at heterozygous state, would not be a rare event. Using the Hardy-Weinberg model, and considering no linkage between the two SNPs, we calculated that up to 25% of the population could show such a haplotype. As a dominant transmission is observed in about 75% of the patients with a *RYR1* mutation (all pathologies included, such as HM and CCD), a unique strategy using the pair of guides presented here could potentially be applied to up to 20% of all the patients with a RyR1-related disease. One restriction is that the second allele should imperatively be fully functional (i.e., only for patients with a dominant mutation and a WT allele). Additionally, it can be proposed that a limited number of gRNA pairs targeting few SNPs have the potential to treat all patients with a dominant form of RyR1-RM. With the rapid evolution of WGS, the SNPs present in each patient could be easily identified, and a limited number of pairs of gRNAs based on the geographic origin of the patients could be developed and tested for each gene to allow deletion of a single allele.

From the five different gRNA pairs designed, only one has proven its efficiency to induce the specific deletion. Different hypotheses can be proposed to explain the absence of deletion: either all the regions of the DNA are not equivalently accessible to Cas9 cleavage, and specifically some intronic regions could be less accessible, or the distance between the two cleavage sites could be important to result in the deletion of the DNA fragment in-between: if too small or too large, the DNA repairs will not result in deletion of the target fragment. In parallel to the manual selection of the SNP/gRNA described here, a dedicated script, so-called "CutOneStrand" has been developed for automated SNP screening and gRNA selection on one allele (https://github.com/clbenoit/CutOneStrand and Supplemental methods). Similar results have been obtained with the manual and the automated selection, the automated selection reducing considerably the time for SNP selection. This script could be used for any of the 571 genes presented in Table S1, in order to induce the specific deletion of one allele, if one allele has been confirmed as sufficient.

The concept of deleting the mutant allele in the case of a dominant pathology has been previously observed using a different methodological approach with siRNA, not only for *RYR1*[12] but also for *DNM2* mutations.[28] In these cases, siRNA was designed to specifically target the mutation.[12,28] The strategy has been further refined and proven efficiency for *DNM2* with siRNA targeting SNPs.[29] This

Figure 4. Molecular characterization of the cells

(A) After mRNA extraction from differentiated myotubes and PCR amplification, the *RYR1* sequence encompassing the mutation c.14387A>G has been sequenced by NGS for the different clones. The electropherograms on the left show the presence of two transcripts in VYC cells, with an "A" and a "G" at the same position, whereas in EC only one transcript with an A is present. The bar graph on the right is a schematic representation based on the quantification of each transcript from NGS data. The relative amount of WT transcript is represented by the upper bar, and the relative amount of mutant transcript is the lower. In all the edited clones, the normal transcript (WT-upper black bar) is expressed in a higher amount (66%) than the mutant transcript (lower blue bar, 33%), whereas in the non-edited clones, as in VYC cells, the two transcripts are observed in equivalent amount (WT, upper black bar 49% and mutant, lower red bar 51%). (B) The analysis of different proteins has been performed using quantitative western blot in CTRL cells, patient's cells VYC, three edited clones (EC-A to C) and three non-edited clones (NEC-A to C). Representative image of three different western blots. (C) Relative amount of myosin/GAPDH confirmed the presence of equivalent amounts of myosin heavy chain (MYHC) and indicates similar differentiation in the different clone. Similar relative amounts of RyR1 protein are also observed in the different clones (RyR1/MYHC amount). Data are presented as the mean ± SEM of the three blots (CTRL and VYC) and for the three edited and the three non-edited clones (EC and NEC). Statistical analysis: one-way ANOVA with Tukey's multiple comparison test, ns: nonsignificant difference. (D) Western blot analysis of Cas9 protein in VYC cells, VYC transduced with lenti-Cas9 (VYC+Cas9) as a positive control, EC-A to -C and NEC-A to -C. This analysis confirms the absence of detectable amount of Cas9 protein in the different clones at the end of the treatment.
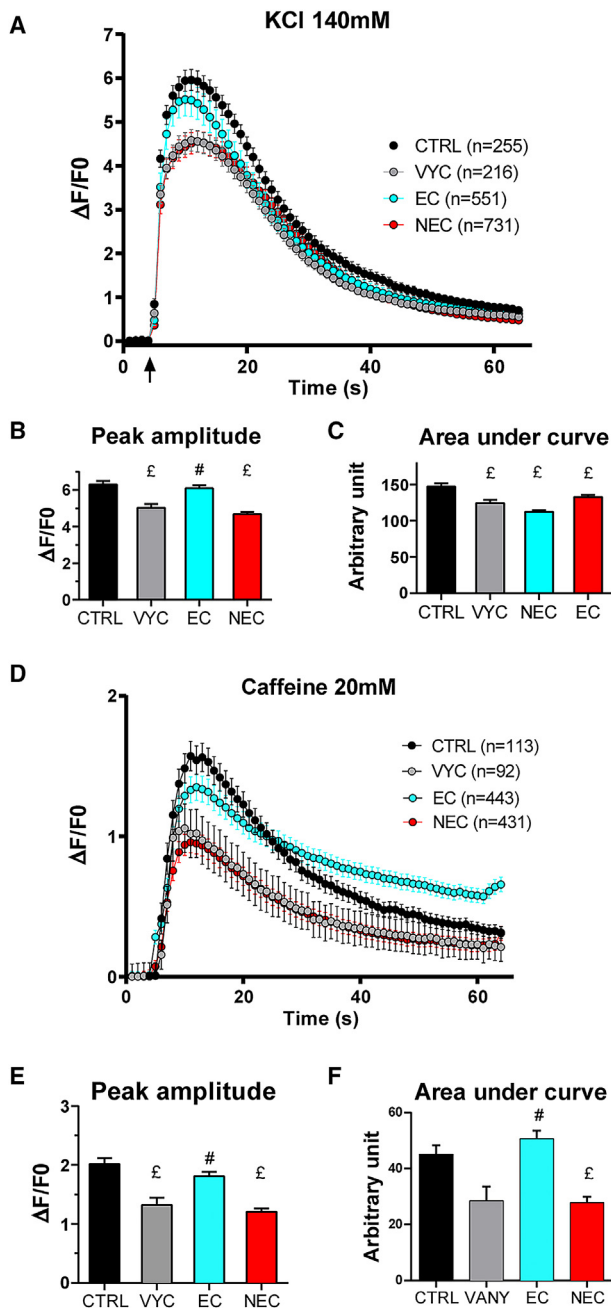
Figure 5. Specificity of the cleavages

(A) Three different types of software were used to identify the putative off-target sites for each gRNA (gRNA1 and gRNA2 for *RYR1*, and g-Killer for *Cas9*): Benchling, CRISPOR, and Cas-OFFinder. For each gRNA, the most probable first 10 to 13 sites predicted by at least two types of software were further selected for PCR amplification and sequencing. (B) For each gRNA, 10 to 13 primer pairs were designed (so-called OT1 to OT13 for gRNA1, OT14 to OT-II3 for gRNA2, and OT-II4 to OT36 for g-Killer, presented in Table 2), and used for PCR amplification of the DNA extracted from the three EC cells (EC-A to -C) and the three NEC cells (NEC-A to -C). Two regions are represented in gray, which correspond to defective PCR amplification (OT11 and OT14, PCR amplification with additional primers also unsuccessful). The PCR fragments were further sequenced and the sequence of each region screened for modification. A green box corresponds to absence of modification, and a red box corresponds to insertion/deletion in the sequence. None of the predicted off-target sites presented any modification. (C) The same procedure (transduction with Lenti-Cas9 and Lenti-G2) was applied to different human immortalized muscle cell lines, which contain the either two selected SNPs (VYC and AB1190) or only one SNP (CTRL), followed by DNA extraction and PCR amplification of the edited zone as in Figure 3C. When the two SNPs are present (VYC and AB1190) the expected deletion can be observed, but when only one SNP is present (CTRL), no deletion is observed.

therapeutic strategy has the potential to be applicable for 75% of RyR1-related disease patients. In the further extension to *in vivo* therapy, the use of viral vectors for the introduction of the CRISPR-Cas9 tools will allow the efficient targeting of all the muscles, even the most difficult muscles for injection, such as respiratory muscles (diaphragm and intercostal muscles). The advantage of such a viral-based approach over the use of nucleic acid molecules such as siRNA or antisense oligonucleotides is the high efficiency and long-term benefit after just a single treatment. The constant improvement of viral vectors for systemic delivery in therapeutic use, increasing the desire tissue targeting (specifically muscle) and reducing the unexpected delivery to other organs such as liver, will increase the efficiency of a viral-based gene therapy,[30] allowing the combination of multiple vectors with preserve efficiency, because each muscle cell will receive all the viral vectors. The progressive deletion of the Cas9 induced by the gRNA against the Cas9 (the "Killer") that can be combined to the other gRNAs under a weaker promoter[23] and injected at the same time can also be used *in vivo* to avoid the long-term expression of Cas9. Alternative methods such as nanoparticles could also be used to introduce the Cas9 as a protein or as mRNA, and not as a DNA, thus limiting the duration of its action to the natural and rapid degradation of protein or mRNA and avoiding the use of the Killer.

The positive impact of deleting the *RYR1* mutant allele has been directly observed in the intensity of calcium release upon stimulation.

Now, the next step will be to translate this observation into muscle strength improvement, which will necessitate *in vivo* testing. The correlation between the amplitude of calcium release in cultured cells and the *in vivo* muscle strength has now to be established. As the patients with a same *RYR1*-dominant mutation have a congenital myopathy of various severity (mild in individual II-8 and more severe in individual IV-2), the efficiency of such a treatment in the context of various severity will have to be considered.

MATERIALS AND METHODS
SNPs identification and gRNA selection
DNA was extracted from blood samples of patients II-8 and IV-1 using the Nucleospin extraction kit (ref. 740952- Macherey-Nagel). Subsequently, WGS was conducted on the DNA of each patient using Illumina HiSeq Analysis Software v2.1. Alignment was obtained by the Isaac aligner (Isaac-04.17.06.15) and variant calling was realized using Isaac variant caller workflow, the reference genome being GRCh38. SNPs from the two genomes were then filtered to retain those found in both patients with a frequency above 1% in the *RYR1* gene and heterozygous. Among the 79 remaining SNPs, only those creating one of the two "G" in an "NGG" PAM were selected, resulting in a list of 14 SNPs. Guide RNAs were then chosen from this list using CRISPOR software[31] (http://crispor.tefor.net). Only the best gRNA matching the following criteria were further utilized: an MIT score of at least 50 out of 100, no predicted OTs for 0 or 1

mismatch, and not classified as inefficient (according to Graf and colleagues[32]). In the end, five SNPs were selected along with their corresponding gRNAs (SNP 1 to 5).

Bioinformatic analysis

A computational pipeline, named CutOneStrand, has been implemented in Bash and Python, using various bioinformatics tools. It integrates a series of scripts to select and analyze SNPs with sequence modifications at PAM sites for CRISPR-Cas9 genome editing. After uploading the sequence of Chr19 containing the *RYR1* gene (GRCh38), the script is designed to identify all the heterozygous SNPs with a frequency >1% and creating or deleting an spCas9 PAM (NGG). The output is a file with the best guides corresponding to these SNPs. The overview of the pipeline is presented in the Supplemental methods.

3D molecular modeling

The molecular modeling has been developed based on the Protein DataBank Entry 7M6L,[33] depicting the open conformation of the RyR1 protein, as the structural template.[34] The mutation modeling was enacted through the Prime software within the Schrodinger Suite, employing the "side chain prediction and residue minimization" protocol.[35] The mutation process adhered to rigorous parameters, including the implementation of the OPLS 2005 forcefield.[36] A 5.0-Å minimization cutoff was applied, coupled with the automatic utilization of conjugate gradient and truncated Newton methods. The minimization protocol, executed with a maximum of two iterations, sought convergence based on a desired final RMS gradient of 0.10, an energy cutoff of 0.100 kcal/mol, and a maximum of 65 truncated Newton iterations per step.

Following the mutation procedure, the structural ramifications were quantified through key metrics. Delta energy and Delta SASA were computed, elucidating shifts in energetic stability and

corded for 1 min. The curves represent the mean ± SEM of fluorescence variation of the *n* different myotubes in each condition. (B) Peak amplitude of calcium release after KCl stimulation presented as mean ± SEM of the maximum for each myotube. Statistical analysis: ANOVA with Tukey's multiple comparison test. *p* value compared with CTRL: VYC *p* = 0.0004, EC *p* = 0.8588, NEC *p* < 0.0001. *p* value compared with VYC: EC *p* = 0.0008, NEC *p* = 0.5398. £: significantly different from CRTL; #: significantly different from VYC. (C) Mean area under the curve presented as mean ± SEM of the AUC for each myotube. Statistical analysis: ANOVA with Tukey's multiple comparison test. *p* value compared with CTRL: VYC *p* = 0.0003, EC *p* = 0.0366, NEC *p* = 0.0025. *p* value compared with VYC: EC *p* = 0.1168, NEC *p* = 0.4021. £: significantly different from CRTL. (D) Kinetics of calcium release upon stimulation by caffeine 20 mM. (E) Peak amplitude of calcium release after caffeine stimulation presented as mean ± SEM of the maximum for each myotube. Statistical analysis: ANOVA with Tukey's multiple comparison test. *p* value compared with CTRL: VYC *p* = 0.0011, EC *p* = 0.4390, NEC *p* < 0.0001. *p* value compared with VYC: EC *p* = 0.0077, NEC *p* = 0.8829. £: significantly different from CRTL; # significantly different from VYC. (F) Mean area under the curve presented as mean ± SEM of the AUC for each myotube. Statistical analysis: ANOVA with Tukey's multiple comparison test. *p* value compared with CTRL: VYC *p* = 0.0925, EC *p* = 0.7287, NEC *p* = 0.0074. *p* value compared with VYC: EC *p* = 0.0009, NEC *p* = 0.9995. £: significantly different from CRTL; #: significantly different from VYC.

Figure 6. Functional characterization of the cells
Fluo-4 calcium imaging performed on myotubes produced from CTRL, VYC, EC, or NEC cell lines. The curves represent the fluorescence variation in CTRL myotubes (black curve), VYC myotubes (gray curve), EC myotubes (blue curve), and NEC myotubes (red curve). All values are presented as mean ± standard error of mean (SEM) of n myotubes. In each condition, *n* = 180 to 255 myotubes have been analyzed, from at least three different experiments (exact number indicated for each curve). The values from the three EC and the three NEC lines have been pooled to simplify the presentation. The curves for each clone are presented individually in Figure S1. (A) Kinetics of calcium release upon stimulation by KCl 140 mM. The stimulation is performed at 5s (arrow), and the fluorescence variation (ΔF/F0) re-

Table 2. Primers for off-target PCR amplifications

Primers	Sequence (5′-3′)	Amplicon (bp)	Genomic coordinates	Comments
OT1_F	GTAACTCCATGTGTATCCCACC	278	chr8:56,538,425-56,538,447	intron:RP11-17A4.3
OT1_R	ACTGAAATTGTGCTCACTTCC			
OT-II_F	TGCTGCTGGTTATTCAAGAC	391	chr1:33,689,212-33,689,234	intron:CSMD2
OT-II_R	GTCTGGATGGCTTCTTGGAG			
OT3_F	CTGTGGTCTCTGAATCGTTTGTC	316	chr22:50,714,785-50,714,807	intron:SHANK3
OT3_R	CATCTCGTCCAGCTTCTCTG			
OT4_F	CTTTCTTCACAGAGCAAAGCA	381	chr2:180,742,621-180,742,643	intergenic:SCHLAP1-RP11-739A13.1
OT4_R	AAATAATGGAGGTGATTCAGGG			
OT5_F	CCTGTTGATTAATTGTGCTCATGG	295	chr3:170,638,699-170,638,721	intergenic:SLC7A14-RP11-373E16.3
OT5_R	GGTGTTTAGTTGAAATGTCCTGTC			
OT6_F	ACATGCACATCTCCTACGTC	298	chr8:20,310,621-20,310,643	intergenic:LZTS1-RP11-563N12.2
OT6_R	TGAGCAGAGCACTTCAAATCC			
OT7_F	GCTCAGAGGCTCAGATTGGA	364	chr8:118,967,897-118,967,919	intergenic:TNFRSF11B-RNU6-12P
OT7_R	GTCATGTCCTCTTCTTGCAC			
OT8_F	ACATTATCGGTAAAGACAGCAG	429	chr20:49,696,619-49,696,641	intron:B4GALT5
OT8_R	CTGTGTCATCAGAAACATTCCA			
OT9_F	CTCATGCTCAGTGATATGCTAGG	278	chr20:63,618,673-63,618,695	intron:GMEB2
OT9_R	CTAACATTTGCCCAAACTGCC			
OT10_F	ACTCCATGAACTCCTAACCA	1393	chr12:128,404,653-128,404,675	exon:RP11-553N19.1
OT10_R	CAAATGTCTTTCCTCTTACTCCAG			
OT11_F	AGCCTGGGTAACAGAGTGAG	302	chrX:40,246,870-40,246,892	intergenic:BCOR-RP11-320G24.1
OT11_R	AGGAGTTTGAGACCAGCCAG			
OT12_F	GGGTGAACATTATGAAGAAGGAC	320	chrX:150,370,131–150,370,153	intron:MAMLD1
OT12_R	TTTCCTGCCATACAGTTGAC			
OT13_F	TATGTTGCAAATGAGGAGACTG	321	chr3:171,944,700-171,944,722	intergenic:TMEM212-AS1-AC055714.1
OT13_R	ACAAATGTCACTGAGAACACAGG			
OT14_F	TTTGGAACCCAGAATACCCAC	337	chr6:154,616,615-154,616,637	intergenic:CNKSR3-SCAF8
OT14_R	AGGCTGGTCTTGAACTCCTG			
OT15_F	AAGTCCCAATCCTTCAATCTACAC	381	chr5:73,820,625-73,820,647	intergenic:ARHGEF28-RNU7-196P
OT15_R	CATAAATCCCGAAGCCCTCTG			
OT16_F	TTTCTGGTGGGATGTTCCTG	441	chr1:147,904,646-147,904,668	intergenic:RP11-433J22.3-GJA8
OT16_R	CCATGTCTTTCTATACTCTAAGCC			
OT17_F	TAGGGAAAGGAGTTATGACGG	311	chr2:26,654,759-26,654,781	intergenic:CIB4-AC015977.6
OT17_R	CTGTGTCCTCTACCCACCTC			
OT18_F	CCAAATTAAGTCTGTCTTCTAGCC	437	chr2:59,534,417-59,534,439	intergenic:AC007179.2-AC007006.1
OT18_R	TTTAACCTCCCAACATATCCGA			
OT19_F	GTGAATTTCTTCATCTGTCAGTGG	317	chr4:170,697,795-170,697,817	intergenic:RP11-789C1.2-RP11-322J23.1
OT19_R	GTTGCTTTGGGTGTTGAGAG			
OT-II0_F	TGTCTAAATCTCACCTTCTTCCAC	322	chr6:30,916,673-30,916,695	intron:VARS2
OT-II0_R	AAACACTTCCCAAGCACTTCC			
OT-II1_F	GGGCTCCTGAGAAATTCCTC	421	chr19:10,009,705-10,009,727	intron:COL5A3
OT-II1_R	GTGGTTATGCGTGTGATTGTG			
OT-II2_F	AGAGACCCTGTATTGGAGAC	294	chr8:137,730,225-137,730,247	intergenic:RNU6-144P-RP11-238K6.1
OT-II2_R	TATCTAGACAGTTCCAAACCCAG			

(Continued on next page)

Table 2. Continued

Primers	Sequence (5'-3')	Amplicon (bp)	Genomic coordinates	Comments
OT-II3_F	CAAGAACTCCCTCCTCCCAG	222	chr8:143,572,268-143,572,290	intron:MROH6
OT-II3_R	TGTGGATGGTAGGTGGAAGG			
OT-II4_F	GTAATATGGCCATGATCCCAC	330	chr5:54,766,221-54,766,243	intergenic:CTD-2591A1.1-AC112198.2
OT-II4_R	GTTGCTACCTGAATAGAATGACAC			
OT-II5_F	TATATGTGGGTTTCGTGTTAGG	298	chr2:53,225,888-53,225,910	intergenic:AC010967.2-AC069157.2
OT-II5_R	ACTGCTGCTTTCTTTACTCTG			
OT-II6_F	CGATTGAAGGGTTTCTTGCTG	367	chr4:104,886,734-104,886,756	intergenic:AC004053.2-RP11-556I14.2
OT-II6_R	TGATAAGCTGGATACTAAGGAGG			
OT-II7_F	CTTGCTTTCTCCAGTGAGCC	280	chr10:112,557,827-112,557,849	intergenic:VTI1A-MIR4295
OT-II7_R	GTAGGAAGCCCTTTCAAACCA			
OT-II8_F	GCCATCTCAGTCTTCCAACC	237	chr5:10,920,923-10,920,945	intergenic:CTD-2154B17.1-CTNND2
OT-II8_R	ACATTGCTTAGGCCAAATCAG			
OT-II9_F	CAAAGGGAGGTTACACAGGA	322	chr7:25,768,926-25,768,948	intergenic:AC003090.1-CTD-2227E11.1
OT-II9_R	CCACTTGTATGCCCACAGAC			
OT30_F	TATGGATAAGGAAAGTGCCGA	377	chr12:53,055,605-53,055,627	exon:TNS2
OT30_R	CTTGCCCTTGTTTCCCTGAC			
OT31_F	CACCCAAGTCCACCTTTCTC	317	chr16:35,441,620-35,441,642	intergenic:LINC01566-RP11-80F22.14
OT31_R	ATGTAGTCCTGATTCAGTTTCCGA			
OT32_F	TATCCTAGAGCTGGAGGAGAG	259	chr16:67,888,669-67,888,691	intergenic:EDC4/CTC-479C5.10/NRN1L-PSKH1
OT32_R	ATTGAACCCTTACTATGTGCTG			
OT33_F	GTACATAGCTCCCAGACAACC	238	chr9:69,297,261-69,297,283	intron:BANCR
OT33_R	GCAAGAAAGGAACTAGCTCAC			
OT34_F	CTGACATGATAAATGGTCCGCT	370	chrX:120,026,774-120,026,796	intergenic:GS1-421I3.2-RP4-755D9.1
OT34_R	CACGGGAATATCCAGAGGGAG			
OT35_F	GCCAGAATGATGTCTCCCAG	349	chr11:62,690,175-62,690,197	intergenic:LRRN4CL-HNRNPUL2-BSCL2/BSCL2
OT35_R	CACTTTCCCACCTGACTCCT			
OT36_F	GACAAAGAATGCACGTAACACC	333	chr13:21,739,618-21,739,640	intergenic:FGF9-RN7SL766P
OT36_R	ACGCCACAGATGTTTATTTCC			

solvent-accessible surface area. The mutation process culminated in the generation of a distinct structural configuration, encapsulating cumulative mutational effects. To enhance result interpretation, PyMol, an integral visualization tool within the Schrodinger Suite, was employed http://www.pymol.org/pymol.[37] This facilitated a comparative analysis between the original and mutated structures, with particular focus on the spatial relationship between alanine 4566 and tyrosine-cysteine 4795. Distance measurements within PyMol provided quantitative insights into the conformational disparities induced by the mutations, thus enriching the structural characterization.

Plasmids and lentiviruses transduction
Lentiviruses were produced by a triple transfection of HEK 293T cells. Lenti-guide encoding gRNA against the chosen SNPs (Lenti-G) or the Cas9 gene (Lenti-Killer, as described by Merienne and colleagues[23]) were produced using Addgene plasmid #87919. Lenti-Cas9 encoding Cas9 was produced from Addgene plasmid #87904. The immortalized myoblasts were transduced in proliferation medium with the two lentiviruses Lenti-G and Lenti-Cas9 at a multiplicity of infection (MOI) of 10, and 7 days later the Cas9 action was stopped by transduction with Lenti-Killer (MOI 20) as described previously.[22]

Cell culture and differentiation
HEK293T cells were maintained in medium composed of Dulbecco's modified Eagle's medium (DMEM) high-glucose pyruvate, supplemented with 10% fetal bovine serum (Life Technologies) and 2% penicillin/streptomycin (Life Technologies).

Investigations on patient material were performed after signature of an informed consent according to the French regulation and have received approval from the local ethical committee (Comite de Protection des Personnes-Sud-Est, France). Immortalized human satellite cells (myoblasts) have been produced as described previously[19] from a 25 years control individual (CTRL[38]) or from a muscle biopsy of patient II-8 (so-called here V-Y4796C or VYC cells). The myoblasts were amplified in proliferation medium composed of Ham's

F-10 (Life Technologies) supplemented with 20% fetal bovine serum (FBS) (Life Technologies), 2% Ultroser G (Pall- Sartorius), and 2% Penicillin-Streptomycin (Life Technologies). Differentiation into myotubes was induced by a shift to differentiation medium: DMEM low glucose (Life Technologies) supplemented with 2% heat-inactivated horse serum (Life Technologies) and 1% penicillin-streptomycin. Myoblasts were amplified in proliferation medium composed of F-10 nutrient medium (Ham's F10) supplemented with 20% FBS, 2% Ultroser G serum, and 2% penicillin/streptomycin. Myoblasts are kept at a confluence 50%–60% max.

Cellular cloning

After trypsination, the myoblasts have been diluted in proliferation medium at 10 cells/mL and seeded at one cell/well in 96-well plates containing 100 μL/well of proliferation medium. During 2 to 6 weeks, the clones have been progressively amplified to larger plates until reaching at least a 35-mm plate, while maintaining the confluency of the myoblasts below 50%.

DNA and RNA extraction on cultured cells

The cells have been collected with TrypLE (ref. 12605-010, Life Technologies) and DNA extracted with the Nucleospin tissue kit following the manufacturer's recommendations (ref. 740952, Macherey-Nagel) for a large amount of cells (300,000 cells). For a smaller amount of cells (ie, during clone selection), the following classical protocol has been used for DNA purification. The cells have been lysed in 500 μL lysis buffer supplemented with proteinase K 100 μg/mL (Tris/HCl 10 mM pH = 7.5, EDTA 10 mM, NaCl 10 mM, N-lauryl sarcosine 0.5% + 100 μg/mL proteinase K). After 2 h at 60°C, DNA was precipitated by addition of 1.5 mL of precipitation buffet (NaCl 150 mM-EtOH 100%), collected by centrifugation and washed with EtOH 70%.

RNA has been extracted from myotubes differentiated for 7 days using Trizol (Life Technologies) followed by chloroform/isoamyl alcohol (49:1 v/v). RNA has been retro-transcribed to cDNA using oligo-dT and transcriptor reverse transcriptase (Roche) according to the manufacturer's recommendations.

DNA and RNA analysis

PCR amplification of the DNA has been performed with Phusion high-fidelity master mix with GC buffer (ref F532L, ThermoFisher). The primers for PCR amplification have been selected with Perl-Primer.[39] The different primer pairs are presented in Table 1.

If a sequencing was further needed, after separation on a 1% agarose gel, the bands of interest were excised and purified with the gel and PCR clean up (ref. 740609, Macherey-Nagel) with a final elution volume of 20 μL, and submitted to Sanger sequencing (Eurofins Genomics).

Total *RYR1* transcripts were amplified as seven overlapping PCR products.[40] They were sequenced after fragmentation and library preparation using NEBNEXT NGS workflow (New England Biolabs)

according to manufacturer recommendation. The library was then sequenced on an S5 IonTorrent platform (ThermoFisher). FastQ files were analyzed using nf-core pipeline (nf-core/rnaseq v3.0), alignments and splice junctions were produced using RNAStar.

Protein analysis

Myoblasts (200,000) were seeded on a laminin-coated 35-mm culture dish and differentiated for 7 days as described previously.[22] The proteins were collected by cell lysis in RIPA (25 mM Tris-HCl, pH 7.6, 150 mM NaCl, 1% NP-40, 1% sodium deoxycholate, 0.1% SDS) with protease inhibitors (200 mM phenylmethylsulfonyl fluoride, and 1 mM diisopropyl fluorophosphate). Protein quantification was performed using BCA kit (Pierce), and 20 μg was loaded in each well of a 5%–15% acrylamide gel for western blot analysis. The amount of RyR1 compared with MYHC as a marker of differentiation was estimated using quantitative western blot, as described before,[22] using a rabbit polyclonal antibody against RyR1[24] and a monoclonal anti-MYHC antibody (MF20, DSHB, Iowa City, IA). Antibody against GAPDH was used as a loading control (anti-GAPDH [14C10] rabbit mAb, Cell Signaling Technology). The presence of the Cas9 protein was tested using antibody against the V5 tag (ref R960-25, Invitrogen). Secondary antibodies used for western blot were labeled with horseradish peroxidase (Jackson Immuno Research). Signal quantification was performed using a ChemiDoc Touch apparatus (Bio-Rad) and the Image Lab software (Bio-Rad). The amount of the chosen protein in each sample was corrected for differences in loading using the amount of GAPDH.

Calcium imaging

Human myotubes (CTRL cells, V-Y4796C cells, three ECs EC-A, EC-B, and EC-C and three NECs NEC-A, NEC-B, NEC-C) were cultured for 7 to 8 days before intracellular calcium measurements. Changes in intracellular calcium were measured on the cultured myotubes, as described previously,[41] using the calcium-dependent fluorescent dye Fluo 4-Direct (Molecular Probes) diluted in differentiation medium. Calcium imaging was performed in Krebs buffer (136 mM NaCl, 5 mM KCl, 2 mM $CaCl_2$, 1 mM $MgCl_2$, 10 mM HEPES, pH 7.4). KCl stimulation (140 mM final concentration) was performed by application of Krebs in which NaCl was replaced by KCl (140 mM KCl, 2 mM $CaCl_2$, 1 mM $MgCl_2$, 10 mM HEPES, pH 7.4). Caffeine was diluted at 20 mM final concentration in Krebs. The curves represent the mean ± SEM of fluorescence variation after stimulation during 65 s of the n myotubes in each condition, from at least three different experiments. The peak amplitude is the mean ± SEM of the maximal amplitude of each myotube (n myotubes in the same condition, from three different experiments), and the area under the curve (AUC) is the mean ± SEM of the area under the fluorescence curve for each myotube.

Statistics

The statistical analysis has been done with GraphPad Prism 6.0 software. The number of samples and the name of the parametric test applied are indicated in each figure legend. Results are considered as significant when $p < 0.05$, the exact value for p being indicated in

the text or figure legends, and significant results are labeled on the graphs whatever the exact *p* value. All data are shown as mean ± SEM.

DATA AND CODE AVAILABILITY
The data are available upon reasonable request to the corresponding author.

SUPPLEMENTAL INFORMATION
Supplemental information can be found online at https://doi.org/10.1016/j.omtn.2024.102259.

AUTHOR CONTRIBUTIONS
M.B., J.F., J.R., and I.M. conceived and designed the study. M.B., M.M., and J.B. conducted the experiments and analyzed the results. C.B. and N.D. conducted bioinformatics and structural analyses. K.M. produced the immortalized myoblasts. N.B.R., A.F.D.-L., and S.Q.-R. recruited the patients, collected blood and muscle samples, and analyzed the patients' phenotype. I.M. wrote the manuscript. J.F. provided expert feedback. All authors contributed to manuscript review.

DECLARATION OF INTERESTS
The authors declare no competing interests.

REFERENCES

1. Marty, I., and Fauré, J. (2016). Excitation-contraction coupling alterations in myopathies. J. Neuromuscul. Dis. *3*, 443–453.

2. Lawal, T.A., Todd, J.J., and Meilleur, K.G. (2018). Ryanodine Receptor 1-Related Myopathies: Diagnostic and Therapeutic Approaches. Neurotherapeutics *15*, 885–899.

3. Lawal, T.A., Todd, J.J., Witherspoon, J.W., Bönnemann, C.G., Dowling, J.J., Hamilton, S.L., Meilleur, K.G., and Dirksen, R.T. (2020). Ryanodine receptor 1-related disorders: an historical perspective and proposal for a unified nomenclature. Skeletal Muscle *10*, 32.

4. Beaufils, M., Travard, L., Rendu, J., and Marty, I. (2022). Therapies for RYR1-Related Myopathies: Where We Stand and the Perspectives. Curr. Pharmaceut. Des. *28*, 15–25.

5. Robinson, R., Carpenter, D., Shaw, M.A., Halsall, J., and Hopkins, P. (2006). Mutations in RYR1 in malignant hyperthermia and central core disease. Hum. Mutat. *27*, 977–989.

6. Amburgey, K., Bailey, A., Hwang, J.H., Tarnopolsky, M.A., Bonnemann, C.G., Medne, L., Mathews, K.D., Collins, J., Daube, J.R., Wellman, G.P., et al. (2013). Genotype-phenotype correlations in recessive RYR1-related myopathies. Orphanet J. Rare Dis. *8*, 117.

7. Richards, S., Aziz, N., Bale, S., Bick, D., Das, S., Gastier-Foster, J., Grody, W.W., Hegde, M., Lyon, E., Spector, E., et al. (2015). Standards and guidelines for the interpretation of sequence variants: a joint consensus recommendation of the American College of Medical Genetics and Genomics and the Association for Molecular Pathology. Genet. Med. *17*, 405–424.

8. Ogasawara, M., and Nishino, I. (2021). A review of core myopathy: central core disease, multiminicore disease, dusty core disease, and core-rod myopathy. Neuromuscul. Disord. *31*, 968–977.

9. Litman, R.S., Griggs, S.M., Dowling, J.J., and Riazi, S. (2018). Malignant Hyperthermia Susceptibility and Related Diseases. Anesthesiology *128*, 159–167.

10. Marty, I., Beaufils, M., Fauré, J., and Rendu, J. (2023). Gene therapies for RyR1-related myopathies. Curr. Opin. Pharmacol. *68*, 102330.

11. Rendu, J., Brocard, J., Denarier, E., Monnier, N., Piétri-Rouxel, F., Beley, C., Roux-Buisson, N., Gilbert-Dussardier, B., Perez, M.J., Romero, N., et al. (2013). Exon skipping as a therapeutic strategy applied to an RYR1 mutation with pseudo-exon inclusion causing a severe core myopathy. Hum. Gene Ther. *24*, 702–713.

12. Loy, R.E., Lueck, J.D., Mostajo-Radji, M.A., Carrell, E.M., and Dirksen, R.T. (2012). Allele-specific gene silencing in two mouse models of autosomal dominant skeletal myopathy. PLoS One *7*, e49757.

13. Anzalone, A.V., Koblan, L.W., and Liu, D.R. (2020). Genome editing with CRISPR-Cas nucleases, base editors, transposases and prime editors. Nat. Biotechnol. *38*, 824–844.

14. Chemello, F., Chai, A.C., Li, H., Rodriguez-Caycedo, C., Sanchez-Ortiz, E., Atmanli, A., Mireault, A.A., Liu, N., Bassel-Duby, R., and Olson, E.N. (2021). Precise correction of Duchenne muscular dystrophy exon deletion mutations by base and prime editing. Sci. Adv. *7*, eabg4910.

15. Happi Mbakam, C., Rousseau, J., Tremblay, G., Yameogo, P., and Tremblay, J.P. (2022). Prime Editing Permits the Introduction of Specific Mutations in the Gene Responsible for Duchenne Muscular Dystrophy. Int. J. Mol. Sci. *23*, 6160.

16. Godbout, K., Rousseau, J., and Tremblay, J.P. (2023). Successful Correction by Prime Editing of a Mutation in the *RYR1* Gene Responsible for a Myopathy. Cells *13*, 31.

17. Monnier, N., Romero, N.B., Lerale, J., Nivoche, Y., Qi, D., MacLennan, D.H., Fardeau, M., and Lunardi, J. (2000). An autosomal dominant congenital myopathy with cores and rods is associated with a neomutation in the RYR1 gene encoding the skeletal muscle ryanodine receptor. Hum. Mol. Genet. *9*, 2599–2608.

18. Rosenberg, H., Pollock, N., Schiemann, A., Bulger, T., and Stowell, K. (2015). Malignant hyperthermia: a review. Orphanet J. Rare Dis. *10*, 93.

19. Mamchaoui, K., Trollet, C., Bigot, A., Negroni, E., Chaouch, S., Wolff, A., Kandalla, P.K., Marie, S., Di Santo, J., St Guily, J.L., et al. (2011). Immortalized pathological human myoblasts: Towards a universal tool for the study of neuromuscular disorders. Skeletal Muscle *1*, 34.

20. Monnier, N., Marty, I., Faure, J., Castiglioni, C., Desnuelle, C., Sacconi, S., Estournet, B., Ferreiro, A., Romero, N., Laquerriere, A., et al. (2008). Null mutations causing depletion of the type 1 ryanodine receptor (RYR1) are commonly associated with recessive structural congenital myopathies with cores. Hum. Mutat. *29*, 670–678.

21. Cacheux, M., Blum, A., Sébastien, M., Wozny, A.S., Brocard, J., Mamchaoui, K., Mouly, V., Roux-Buisson, N., Rendu, J., Monnier, N., et al. (2015). Functional characterization of a Central Core Disease RyR1 mutation (p.Y4864H) associated with quantitative defect in RyR1 protein. J. Neuromuscul. Dis. *2*, 421–432.

22. Beaufils, M., Tourel, A., Petiot, A., Halmai, N.B., Segal, D.J., Rendu, J., and Marty, I. (2022). Development of knock-out muscle cell lines using lentivirus-mediated CRISPR/Cas 9 gene editing. J. Vis. Exp. *16*, 184.

23. Merienne, N., Vachey, G., de Longprez, L., Meunier, C., Zimmer, V., Perriard, G., Canales, M., Mathias, A., Herrgott, L., Beltraminelli, T., et al. (2017). The Self-Inactivating KamiCas9 System for the Editing of CNS Disease Genes. Cell Rep. *20*, 2980–2991.

24. Marty, I., Robert, M., Villaz, M., De Jongh, K., Lai, Y., Catterall, W.A., and Ronjat, M. (1994). Biochemical Evidence for a complex involving Dihydropyridine Receptor and Ryanodine Receptor in Triad Junctions of Skeletal Muscle. Proc. Natl. Acad. Sci. USA *91*, 2270–2274.

25. Takeshima, H., Iino, M., Takekura, H., Nishi, M., Kuno, J., Minowa, O., Takano, H., and Noda, T. (1994). Excitation-contraction uncoupling and muscular degeneration in mice lacking functional skeletal muscle ryanodine-receptor gene. Nature *369*, 556–559.

26. Pelletier, L., Petiot, A., Brocard, J., Giannesini, B., Giovannini, D., Sanchez, C., Travard, L., Chivet, M., Beaufils, M., Kutchukian, C., et al. (2020). In vivo RyR1 reduction in muscle triggers a core-like myopathy. Acta Neuropathol. Commun. *8*, 192.

27. Christie, K.A., Robertson, L.J., Conway, C., Blighe, K., DeDionisio, L.A., Chao-Shern, C., Kowalczyk, A.M., Marshall, J., Turnbull, D., Nesbit, M.A., and Moore, C.B.T. (2020). Mutation-Independent Allele-Specific Editing by CRISPR-Cas9, a Novel Approach to Treat Autosomal Dominant Disease. Mol. Ther. *28*, 1846–1857.

28. Trochet, D., Prudhon, B., Beuvin, M., Peccate, C., Lorain, S., Julien, L., Benkhelifa-Ziyyat, S., Rabai, A., Mamchaoui, K., Ferry, A., et al. (2018). Allele-specific silencing therapy for Dynamin 2-related dominant centronuclear myopathy. Mol. Med. *10*, 239–253.

29. Dudhal, S., Mekzine, L., Prudhon, B., Soocheta, K., Cadot, B., Mamchaoui, K., Trochet, D., and Bitoun, M. (2022). Development of versatile allele-specific siRNAs able to silence all the dominant dynamin 2 mutations. Mol. Ther. Nucleic Acids *29*, 733–748.

30. Liu, J., Koay, T.W., Maiakovska, O., Zayas, M., and Grimm, D. (2023). Progress in Bioengineering of Myotropic Adeno-Associated Viral Gene Therapy Vectors. Hum. Gene Ther. *34*, 350–364.

31. Concordet, J.P., and Haeussler, M. (2018). CRISPOR: intuitive guide selection for CRISPR/Cas9 genome editing experiments and screens. Nucleic Acids Res. *46*, W242–W245.

32. Graf, R., Li, X., Chu, V.T., and Rajewsky, K. (2019). sgRNA Sequence Motifs Blocking Efficient CRISPR/Cas9-Mediated Gene Editing. Cell Rep. *26*, 1098–1103.e3.

33. wwPDB consortium (2019). Protein Data Bank: the single global archive for 3D macromolecular structure data. Nucleic Acids Res. *47*, D520–D528.

34. Melville, Z., Kim, K., Clarke, O.B., and Marks, A.R. (2022). High-resolution structure of the membrane-embedded skeletal muscle ryanodine receptor. Structure *30*, 172–180.e3.

35. Sankar, K., Trainor, K., Blazer, L.L., Adams, J.J., Sidhu, S.S., Day, T., Meiering, E., and Maier, J.K.X. (2022). A Descriptor Set for Quantitative Structure-property Relationship Prediction in Biologics. Mol. Inform. *41*, e2100240.

36. Jorgensen, W.L., Maxwell, D.S., and Tirado-Rives, J. (1996). Development and testing of the OPLS all-atom force field on conformational energetics and properties of organic liquids. J. Am. Chem. Soc. *118*, 11225–11236.

37. Schrödinger and DeLano. (2020). http://www.pymol.org/pymol.

38. Chivet, M., McCluskey, M., Nicot, A.S., Brocard, J., Beaufils, M., Giovannini, D., Giannesini, B., Poreau, B., Brocard, J., Humbert, S., et al. (2023). Huntingtin regulates calcium fluxes in skeletal muscle. J. Gen. Physiol. *155*, e202213103.

39. Marshall, O.J. (2004). PerlPrimer: cross-platform, graphical primer design for standard, bisulphite and real-time PCR. Bioinformatics *20*, 2471–2472.

40. Garibaldi, M., Rendu, J., Brocard, J., Lacene, E., Fauré, J., Brochier, G., Beuvin, M., Labasse, C., Madelaine, A., Malfatti, E., et al. (2019). 'Dusty core disease' (DuCD): expanding morphological spectrum of RYR1 recessive myopathies. Acta Neuropathol. Commun. *7*, 3.

41. Oddoux, S., Brocard, J., Schweitzer, A., Szentesi, P., Giannesini, B., Brocard, J., Fauré, J., Pernet-Gallay, K., Bendahan, D., Lunardi, J., et al. (2009). Triadin deletion induces impaired skeletal muscle function. J. Biol. Chem. *284*, 34918–34929.